Band Gap Tuning in New Strontium Seleno-Stannates

Abdeljalil Assoud, Navid Soheilnia, and Holger Kleinke*

Department of Chemistry, University of Waterloo, Waterloo, ON, Canada N2L 3G1

Received January 13, 2004. Revised Manuscript Received March 16, 2004

The new ternary seleno-stannates Sr_2SnSe_5 and $SrSn_2Se_4$ were both prepared from directly reacting the elements in stoichiometric ratios at 850 °C, followed by slow cooling. Sr_2SnSe_5 crystallizes in the Eu_2SnSe_5 type with Sn^{IV}, Se^{-II}, and nonlinear Se_3^{2-} units, space group $P2_12_12$, with lattice dimensions of $a = 1205.7(2)$ pm, $b = 1658.3(3)$ pm, $c = 863.9(2)$ pm, $V = 1.7272(6)$ nm^3 ($Z = 8$). $SrSn_2Se_4$ forms a distorted variant of the $SrIn_2Se_4$ type with mixed valences, i.e., Sn^{II} and Sn^{IV} instead of two In^{III}. The distortion is reflected in lowering the symmetry from *Fddd* to *Fdd*2, occurring with differently sized and distorted $Sn^{II}Se_4$ and $Sn^{IV}Se_4$ tetrahedra. The lattice dimensions are $a = 2189.2(1)$ pm, $b = 2189.3(1)$ pm, $c = 1354.70(7)$ pm, $V = 6.4928(6)$ nm^3 ($Z = 32$). The Sn^{II} atoms may be replaced by Mg, producing the new isostructural compound $SrMgSnSe_4$ with $a = 2176.0(1)$ pm, $b = 2185.9(1)$ pm, $c = 1340.60(9)$ pm, $V = 6.3765(7)$ nm^3. $SrMgSnSe_4$ is a red material (indicative of a band gap of 2.0 eV), while the two other seleno-stannates are black, pointing toward gaps <1.7 eV. The computed band gaps are 1.8 eV for $SrMgSnSe_4$, 0.9 eV for Sr_2SnSe_5, and 0.2 eV for $SrSn_2Se_4$.

Introduction

Exploratory thermoelectric researchers concentrate on a number of different materials families, including but not limited to bismuth chalcogenides,[1−5] antimony chalcogenides,[6−16] tin chalcogenides (chalcogeno-stannates),[17,18] and germanium and tin-based clathrates.[19−22] The ideal thermoelectric material is a narrow gap semiconductor crystallizing in a complex yet highly symmetric unit cell with heavy constituent elements,[23,24] and calculations indicate that the band gap should be between 0.1 and 0.6 eV (which is temperature dependent).[25]

Many alkaline and alkaline earth tin sulfides and selenides are known, as well as a few tellurides.[26] Typically, these compounds are colored materials, indicative of band gaps between 1.7 and 3.0 eV. While no Sr seleno-stannates were known before our investigations, the thio-stannate Sr_2SnS_4 was reported in the year 2003 to be "yellow-orange".[27] As we expect the band gaps to occur between the filled p block of the chalcogen and the empty s states of Sn, we anticipate to reduce the gap by broadening the p block by adding polychalcogenide groups. Alternatively, by using mixed valent Sn a small gap could separate filled Sn^{II} s states from empty Sn^{IV} s states.

* To whom correspondence should be addressed. E-mail: kleinke@uwaterloo.ca.

(1) Kanatzidis, M. G.; McCarthy, T. J.; Tanzer, T. A.; Chen, L.-H.; Iordanidis, L.; Hogan, T.; Kannewurf, C. R.; Uher, C.; Chen, B. *Chem. Mater.* **1996**, *8*, 1465−1474.

(2) Chung, D.-Y.; Hogan, T.; Brazis, P.; Rocci-Lane, M.; Kannewurf, C.; Bastea, M.; Uher, C.; Kanatzidis, M. G. *Science (Washington, D.C.)* **2000**, *287*, 1024−1027.

(3) Hsu, K.-F.; Chung, D.-Y.; Lal, S.; Mrotzek, A.; Kyratsi, T.; Hogan, T.; Kanatzidis, M. G. *J. Am. Chem. Soc.* **2002**, *124*, 2410−2411.

(4) Kyratsi, T.; Dyck, J. S.; Chen, W.; Chung, D.-Y.; Uher, C.; Paraskevopoulos, K. M.; Kanatzidis, M. G. *J. Appl. Phys.* **2002**, *92*, 965−975.

(5) Chung, D.-Y.; Jobic, S.; Hogan, T.; Kannewurf, C. R.; Brec, R.; Rouxel, J.; Kanatzidis, M. G. *J. Am. Chem. Soc.* **1997**, *119*, 2505−2515.

(6) Venkatasubramanian, R.; Slivola, E.; Colpitts, T.; O'Quinn, B. *Nature (London)* **2001**, *413*, 597−602.

(7) Chen, J. H.; Dorhout, P. K. *J. Alloys Compd.* **1997**, *249*, 199−205.

(8) Choi, K.-S.; Chung, D.-Y.; Mrotzek, A.; Brazis, P.; Kannewurf, C. R.; Uher, C.; Chen, W.; Hogan, T.; Kanatzidis, M. G. *Chem. Mater.* **2001**, *13*, 756−764.

(9) Shelimova, L. E.; Karpinskii, O. G.; Konstantinov, P. P.; Kretova, M. A.; Avilov, E. S.; Zemskov, V. S. *Inorg. Mater.* **2001**, *37*, 342−348.

(10) Kyratsi, T.; Dyck, J. S.; Chen, W.; Chung, D.-Y.; Uher, C.; Paraskevopoulos, K. M.; Kanatzidis, M. G. *Mater. Res. Soc. Symp. Proc.* **2002**, *691*, 419−424.

(11) Dhar, S. N.; Desai, C. F. *Philos. Magn. Lett.* **2002**, *82*, 581−587.

(12) Kuznetsov, A. V.; Letyuchenko, S. D.; Motskin, V. V. *J. Thermoelectr.* **2002**, 43−48.

(13) Thonhauser, T.; Scheidemantel, T. J.; Sofo, J. O.; Badding, J. V.; Mahan, G. D. *Phys. Rev.* **2003**, *B68*, 085201/085201−085201/085208.

(14) Dashjav, E.; Szczepenowska, A.; Kleinke, H. *J. Mater. Chem.* **2002**, *12*, 345−349.

(15) Soheilnia, N.; Dashjav, E.; Kleinke, H. *Can. J. Chem.* **2003**, *81*, 1157−1163.

(16) Assoud, A.; Soheilnia, N.; Kleinke, H. *J. Solid State Chem.*, in press.

(17) Mrotzek, A.; Iordanidis, L.; Kanatzidis, M. G. *Inorg. Chem.* **2001**, *40*, 6204−6211.

(18) Mrotzek, A.; Hogan, T.; Kanatzidis, M. G. *Mater. Res. Soc. Symp. Proc.* **2002**, *691*, 101−112.

(19) Blake, N. P.; Mollnitz, L.; Kresse, G.; Metiu, H. *J. Chem. Phys.* **1999**, *111*, 3133−3144.

(20) Chen, F.; Stokes, K. L.; Nolas, G. S. *J. Phys. Chem. Solids* **2002**, *63*, 827−832.

(21) Bentien, A.; Iversen, B. B.; Bryan, J. D.; Stucky, G. D.; Palmqvist, A. E. C.; Schultz, A. J.; Henning, R. W. *J. Appl. Phys.* **2002**, *91*, 5694−5699.

(22) Kitagawa, J.; Sasakawa, T.; Suemitsu, T.; Takabatake, T.; Ishikawa, M. *J. Phys. Soc. Jpn.* **2002**, *71*, 1222−1225.

(23) Rowe, D. M. *CRC Handbook of Thermoelectrics*; CRC Press: Boca Raton, FL, 1995.

(24) DiSalvo, F. J. *Science (Washington, D.C.)* **1999**, *285*, 703−706.

(25) Sofo, J. O.; Mahan, G. D. *Phys. Rev.* **1994**, *B49*, 4565−4570.

(26) Villars, P. *Pearson's Handbook*; Desk Edition; American Society for Metals: Materials Park, OH, 1997.

(27) Pocha, R.; Tampier, M.; Hofmann, R. D.; Mosel, B. D.; Pöttgen, R.; Johrendt, D. *Z. Anorg. Allg. Chem.* **2003**, *629*, 1379−1384.

10.1021/cm0499242 CCC: $27.50
Published on Web 04/20/2004

Because of the similarities between Eu^{II} and Sr^{II}, we turned our attention toward the black selenide Eu_2SnSe_5, which includes Eu^{II}, Sn^{IV}, Se^{-II}, and Se_3^{2-} groups, and an experimentally determined band gap of 1.07 eV.[28] To verify whether the size of the gap depends on the cations, the Eu atoms, we (successfully) attempted to synthesize its Sr analogue to investigate its electronic structure. Furthermore, we tried to replace the two In^{III} atoms of the yellow selenide $SrIn_2Se_4$[29] by Sn^{II} and Sn^{IV}, thereby preparing the analogous but black Sn compound, $SrSn_2Se_4$. To experimentally prove the presence of Sn^{II}, we replaced it with Mg^{II}, and so synthesized the quaternary red selenide $SrMgSnSe_4$. Thus, with this contribution, we introduce three new seleno-stannates, namely, Sr_2SnSe_5, $SrSn_2Se_4$, and $SrMgSnSe_4$, all of them being acentric semiconductors. Preliminary results were presented at a recent ACS meeting.[30]

Experimental Section

Synthesis. The elements were acquired either in big blocks (Sr, 99% nominal purity, ALFA AESAR; Mg, 99.8%, ALFA AESAR) or in powder form (Sn, 99.8%, −325 mesh, ALFA AESAR; Se, 99.5%, −100 mesh, Aldrich). The surface of the Sr block was simply cut off in the inert gas box to keep it as free of oxygen as possible. Sr and Mg were cut into millimeter-sized pieces. All reactions were carried out in evacuated fused silica tubes placed into temperature controlled resistance furnaces, starting from the elements in the respective stoichiometric ratios.

The two silica tubes containing Sr, Sn, and Se in the 2:1:5 and 1:2:4 ratios, respectively, were heated to 850 °C within 24 h, kept at 850 °C for a period of 12 h, and then cooled to the annealing temperature of 650 °C within 2 h. After sintering at 650 °C for 300 h, the furnace with both tubes was allowed to cool to room temperature within 24 h. The samples looked homogeneous, comprising mostly microcrystalline black powder.

The Mg containing silica tube was annealed at 700 °C for 120 h, and then slowly cooled to 150 °C within 200 h. Thereafter, the furnace was switched off to reach room temperature within a few hours. The product appeared to be red. Thus far, all our attempts to synthesize analogous sulfides or tellurides failed.

Analysis. A portion of the reaction products was ground into fine powder for X-ray powder analysis with the INEL powder diffractometer utilizing a position sensitive detector and Cu $K\alpha_1$ radiation. No known materials could be found in any of the three experimentally obtained powder diagrams. Only the desired elements (Sr, Sn, Se, and Mg in the last sample) were detected in the energy dispersive analysis of X-rays using an electron microscope (CAM-SCAN, CS 4DV) with an additional EDX device (detector: NORAN Instruments), i.e., no impurities (e.g., coming from the silica tube, i.e., Si or O) were present. The scans were performed with an acceleration voltage of 25 kV under high dynamic vacuum. The Sr:Sn:Se ratios were calculated to be (averaged over selected crystals) 25:12:63 atom % for Sr_2SnSe_5 and 13:26:61 atom % for $SrSn_2Se_4$. The atom % values expected based on the formulas are 25:12.5:62.5 atom % for Sr_2SnSe_5 and 14.3:28.6:57.1 atom % for $SrSn_2Se_4$.

Structure Determination. From each sample, one block-like single crystal was chosen under an optical microscope for an X-ray single-crystal structure study. The diffraction data were measured with the use of graphite-monochromatized Mo $K\alpha_1$ radiation on a BRUKER Smart APEX CCD diffractometer. The crystal-to-detector distance was 4.547 cm. Data were collected by scans of 0.3° in ω in two groups of 606 frames at $\phi = 0°$ and 60° for each crystal. The exposure times per frame were 30 s for the Sr_2SnSe_5 and $SrMgSnSe_4$ crystals, and 60 s for $SrSn_2Se_4$. The data were corrected for Lorentz and polarization effects. Absorption corrections were based on fitting a function to the empirical transmission surface as sampled by multiple equivalent measurements using SADABS.[31]

Table 1. Crystallographic Data for Sr_2SnSe_5, $SrSn_2Se_4$, and $SrMgSnSe_4$

chemical formula	Sr_2SnSe_5	$SrSn_2Se_4$	$SrMgSnSe_4$
fw [g/mol]	688.73	640.84	546.46
T of measurement [K]	293(2)	293(2)	293(2)
λ [pm]	71.073	71.073	71.073
space group	$P2_12_12$	$Fdd2$	$Fdd2$
a [pm]	1205.7(2)	2189.2(1)	2176.01(1)
b [pm]	1658.3(3)	2189.3(1)	2185.9(2)
c [pm]	863.9(2)	1354.70(7)	1340.60(9)
V [nm^3]	1.7272(6)	6.4928(6)	6.3765(7)
Z	8	32	32
μ [cm^{-1}]	361.56	304.88	280.61
ρ_{calcd} [g/cm^3]	5.297	5.245	4.554
$R(F_o)^a/R_w(F_o^2)^b$	0.042/0.082	0.033/0.099	0.030/0.069

^{a} $R(F_o) = \sum||F_o| - |F_c||/\sum|F_o|$. ^{b} $R_w(F_o^2) = [\sum[w(F_o^2 - F_c^2)^2]/\sum[w(F_o^2)^2]]^{1/2}$.

For Sr_2SnSe_5, we started the structure refinements[32] from the Eu_2SnSe_5 model published by Dorhout et al., which produced satisfying residual factors. The structure of $SrSn_2Se_4$ did not converge well when refining the atomic coordinates of $SrIn_2Se_4$ in the centric space group $Fddd$ ($R(F_o)$, e.g., stayed above 0.15); much better residual factors and thermal displacement parameters were obtained from solving the structure in the acentric space group $Fdd2$, without any suspiciously high correlation factors. We used the latter model to refine $SrMgSnSe_4$ after replacing the two Sn sites with the longer Sn−Se bonds for Mg. This as well produced satisfying residual factors, while a tentative refinement in $Fddd$ failed. The small Flack parameters of 0.04(1) ($SrSn_2Se_4$) and 0.02(1) ($SrMgSnSe_4$) are indicative of the absence of an inversion center.[33] We therefore conclude that $Fdd2$ is indeed the right space group, and both $SrSn_2Se_4$ and $SrMgSnSe_4$ crystallize in the $BaCdSnS_4$ type.[34]

As is standard in our laboratories because of often encountered mixed occupancies and/or deficiencies,[35−40] we refined the occupancies of all metal atoms in all three cases, but found no significant deviations from 100% occupancy. Next, the occupancy factors of the metal atoms were fixed at 100%, and then the Se occupancies were refined. Again, no significant anomalies occurred. Therefore, all occupancy factors were fixed at 100% in the final refinement cycles. Details of the crystallographic investigations are given in Table 1; atomic parameters can be found in Tables 2−4.

Calculations of the Electronic Structure. The electronic structures of the three new selenides Sr_2SnSe_5, $SrSn_2Se_4$, and $SrMgSnSe_4$ were computed, as well as $SrIn_2Se_4$ for comparison, employing the LMTO method (LMTO = linear muffin tin orbitals), which utilizes the atomic spheres approximation (ASA).[41,42] In the LMTO approach, the density functional

(28) Evenson, C. R. I.; Dorhout, P. K. *Z. Anorg. Allg. Chem.* **2001**, *627*, 2178−2182.
(29) Klee, W.; Schäfer, W. *Rev. Chim. Miner.* **1979**, *16*, 465−472.
(30) Kleinke, H. In *Abstracts of Papers*, 226th National Meeting of the American Chemical Society, New York, NY, Sept 7−11, 2003; American Chemical Society: Washington, DC, 2003; INOR-245.
(31) *SAINT*, version 4; Siemens Analytical X-ray Instruments Inc.: Madison, WI, 1995.
(32) Sheldrick, G. M. *SHELXTL*, version 5.12; Siemens Analytical X-Ray Systems: Madison, WI, 1995.
(33) Flack, H. D. *Acta Crystallogr.* **1983**, *A39*, 876−881.
(34) Teske, C. L. *Z. Anorg. Allg. Chem.* **1980**, *460*, 163−168.
(35) Kleinke, H. *J. Am. Chem. Soc.* **2000**, *122*, 853−860.
(36) Kleinke, H. *Can. J. Chem.* **2001**, *79*, 1338−1343.
(37) Kleinke, H. *J. Solid State Chem.* **2001**, *159*, 134−138.
(38) Kleinke, H. *Inorg. Chem.* **2001**, *40*, 95−100.
(39) Elder, I.; Lee, C.-S.; Kleinke, H. *Inorg. Chem.* **2002**, *41*, 538−545.
(40) Bobev, S.; Kleinke, H. *Chem. Mater.* **2003**, *15*, 3523−3529.
(41) Andersen, O. K. *Phys. Rev.* **1975**, *B12*, 3060−3083.

Table 2. Atomic Coordinates and Equivalent Displacement Parameters of Sr_2SnSe_5

atom	Wyckoff site	*x*	*y*	*z*	U_{eq}/Å^2
Sr(1)	*4c*	0.61478(12)	0.82125(8)	0.74554(12)	0.0120(3)
Sr(2)	*4c*	0.61722(12)	0.82066(8)	0.24155(12)	0.0131(3)
Sr(3)	*4c*	0.74571(12)	0.57056(8)	0.75846(13)	0.0134(3)
Sr(4)	*4c*	0.24705(12)	0.92913(8)	0.74037(13)	0.0129(3)
Sn(1)	*4c*	0.44703(6)	0.60337(5)	0.50000(13)	0.0240(2)
Sn(2)	*4c*	0.40725(6)	0.67401(4)	0.01448(10)	0.01248(17)
Se(1)	*4c*	0.61792(8)	0.67455(6)	0.00552(15)	0.0127(2)
Se(2)	*4c*	0.62788(8)	0.68136(6)	0.50496(15)	0.0118(2)
Se(3)	*2a*	1/2	1/2	0.7270(2)	0.0171(5)
Se(4)	*2a*	1/2	1/2	0.2796(2)	0.0148(4)
Se(5)	*4c*	0.75457(8)	0.93024(6)	0.98763(18)	0.0120(2)
Se(6)	*4c*	0.74236(8)	0.92686(6)	0.48675(18)	0.0117(2)
Se(7)	*4c*	0.43900(9)	0.89334(7)	0.98853(17)	0.0180(2)
Se(8)	*4c*	0.44208(9)	0.89143(6)	0.48826(17)	0.0156(2)
Se(9)	*4c*	0.86905(14)	0.76108(8)	0.72304(15)	0.0168(3)
Se(10)	*2b*	1/2	0	0.1567(2)	0.0155(4)
Se(11)	*4c*	0.36665(14)	0.74819(8)	0.76559(14)	0.0149(3)
Se(12)	*2b*	1/2	0	0.65109(19)	0.0145(4)

Table 3. Atomic Coordinates and Equivalent Displacement Parameters of $SrSn_2Se_4$

atom	Wyckoff site	*x*	*y*	*z*	U_{eq}/Å^2
Sr(1)	*8a*	1/2	0	0.51306(14)	0.0121(3)
Sr(2)	*8a*	1/4	1/4	0.76830(13)	0.0120(3)
Sr(3)	*16b*	0.49820(6)	0.25269(3)	0.51406(11)	0.0114(3)
Sn(1)	*16b*	0.42592(4)	0.12519(5)	0.79677(6)	0.02054(19)
Sn(2)	*16b*	0.38735(4)	0.12389(5)	0.26722(6)	0.01938(18)
Sn(3)	*16b*	0.36397(4)	0.12542(4)	0.51706(4)	0.00782(14)
Sn(4)	*16b*	0.56833(4)	0.12543(4)	0.22501(4)	0.00770(15)
Se(1)	*16b*	0.46310(4)	0.12572(7)	0.61620(7)	0.0085(2)
Se(2)	*16b*	0.37222(5)	0.03435(6)	0.89843(10)	0.0108(3)
Se(3)	*16b*	0.37271(5)	0.21595(6)	0.90121(10)	0.0099(3)
Se(4)	*16b*	0.28372(5)	0.12689(7)	0.64769(8)	0.0108(2)
Se(5)	*16b*	0.46830(4)	0.12445(8)	0.12902(7)	0.0094(3)
Se(6)	*16b*	0.37096(6)	0.21454(6)	0.39822(10)	0.0105(3)
Se(7)	*16b*	0.37046(6)	0.03471(6)	0.40155(10)	0.0106(3)
Se(8)	*16b*	0.53588(4)	0.12698(7)	0.40266(8)	0.0086(2)

Table 4. Atomic Coordinates and Equivalent Displacement Parameters of $SrMgSnSe_4$

atom	Wyckoff site	*x*	*y*	*z*	U_{eq}/Å^2
Sr1	*8a*	1/2	0	0.51490(14)	0.0161(4)
Sr2	*8a*	1/4	1/4	0.76912(14)	0.0160(4)
Sr3	*16b*	0.49804(4)	0.25274(3)	0.51538(12)	0.0158(4)
Mg1	*16b*	0.42622(14)	0.12543(17)	0.8000(2)	0.0207(6)
Mg2	*16b*	0.38822(14)	0.12353(17)	0.2684(2)	0.0214(6)
Sn3	*16b*	0.36485(3)	0.12537(3)	0.51578(5)	0.01154(13)
Sn4	*16b*	0.56933(3)	0.12512(3)	0.22542(4)	0.01225(13)
Se1	*16b*	0.46233(4)	0.12566(7)	0.62050(6)	0.0121(2)
Se2	*16b*	0.37358(4)	0.03561(5)	0.89529(10)	0.0145(3)
Se3	*16b*	0.37409(4)	0.21482(5)	0.89790(11)	0.0147(3)
Se4	*16b*	0.28174(4)	0.12685(7)	0.64416(7)	0.01586(18)
Se5	*16b*	0.46770(3)	0.12417(7)	0.13308(7)	0.0144(2)
Se6	*16b*	0.37340(5)	0.21300(5)	0.39399(10)	0.0153(3)
Se7	*16b*	0.37247(5)	0.03538(5)	0.39799(11)	0.0148(3)
Se8	*16b*	0.53951(4)	0.12674(7)	0.40526(7)	0.01411(17)

theory is used with the local density approximation (LDA).[43] The integrations in *k* space were performed by an improved tetrahedron method[44] on grids of more than 150 independent *k* points of the first Brillouin zone, depending on its size and symmetry.

Results and Discussion

The Polyselenide Sr_2SnSe_5. This Sr compound is isotypic with Eu_2SnSe_5, the crystal structure of which was described in detail in 2001.[28] The structure of Sr_2SnSe_5 is depicted in Figure 1. The almost isotropic increase of the cell dimensions stems from larger Sr−Se distances, ranging from 312 to 337 pm, compared to the range of 308−332 pm for the nine Eu−Se distances.

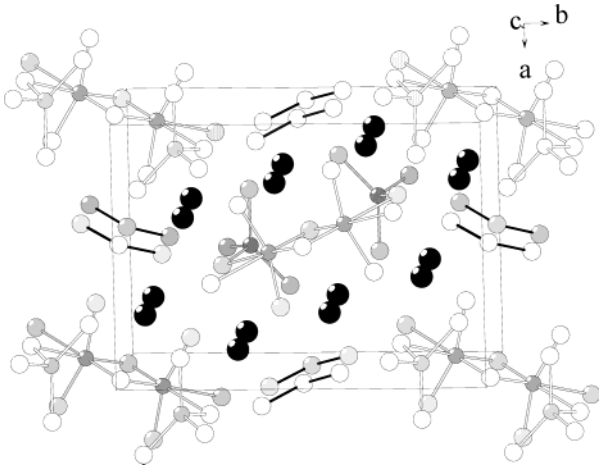

Figure 1. Projection of the structure of Sr_2SnSe_5 along the *c* axis. Black circles: Sr. Gray: Sn. White: Se. Different heights are reflected in different shading; Sr−Se bonds are omitted for clarity.

Table 5. Selected Interatomic Distances [pm] of Sr_2SnSe_5

Sn(1)−Se(6)	252.07(13)	Sn(2)−Se(11)	252.52(15)
Sn(1)−Se(2)	253.55(12)	Sn(2)−Se(5)	252.53(12)
Sn(1)−Se(4)	264.06(16)	Sn(2)−Se(1)	254.11(12)
Sn(1)−Se(3)	268.18(17)	Sn(2)−Se(9)	255.19(16)
Sn(1)−Se(9)	310.6(2)	Se(7)−Se(10)	240.43(17)
Sn(1)−Se(11)	346.0(2)	Se(8)−Se(12)	238.91(16)

Two crystallographically nonlinear Se_3 units are packed on top of each other along the *c* axis, with typical Se−Se bonds of 239 and 240 pm (Eu_2SnSe_5: 240 and 242 pm). These values compare well with bent Se_3^{2-} groups, e.g., in K_2Se_3 (238 pm),[45] Rb_2Se_3 (238 pm), and Cs_2Se_3 (235 pm).[46] Thus, an assignment of two negative charges for each Se_3 group is justified. Assuming the typical oxidation states of +II for Sr, and −II for the other Se atoms, both symmetry independent Sn atoms should be tetravalent, according to the formula $(Sr^{II})_4(Sn^{IV})_2(Se^{-II})_7Se_3^{2-}$.

The Sn(2) atom exhibits the (distorted) tetrahedral coordination sphere expected for Sn^{IV}, with typical Sn−Se distances of 253−255 pm (Eu_2SnSe_5: 252−256 pm). Details are given in Table 5. Similar distances for tetracoordinated Sn^{IV} atoms occur in the isolated $SnSe_4$ tetrahedra of K_4SnSe_4 (249−253 pm).[47]

On the other hand, the Sn(1) is surrounded by six Se atoms in a peculiar fashion, with two short distances (252 and 254 pm), two intermediate ones (264 and 268 pm), a long one (311 pm), and a very long one of 346 pm. The last one is not likely to be of significant bonding character, but the 311 pm contact probably is, causing an increase in the average of the four bonds <300 pm by almost 6 pm (259.5 pm), compared to the average of the Sn(2)−Se bonds (253.6 pm). Furthermore, the 311 pm distance is opposite to the 268 pm distance, thus possibly directly responsible for its enlarged length. As the 346 pm distance is opposite to the 264 pm distance,

(42) Skriver, H. L. *The LMTO Method*; Springer: Berlin, Germany, 1984.
(43) Hedin, L.; Lundqvist, B. I. *J. Phys.* **1971**, *4C*, 2064−2083.
(44) Blöchl, P. E.; Jepsen, O.; Andersen, O. K. *Phys. Rev.* **1994**, *B49*, 16223−16233.
(45) Böttcher, P. *Z. Anorg. Allg. Chem.* **1977**, *432*, 167−172.
(46) Böttcher, P. *Z. Anorg. Allg. Chem.* **1980**, *461*, 13-21.
(47) Klepp, K. O. *Z. Naturforsch.* **1992**, *47B*, 411−417.

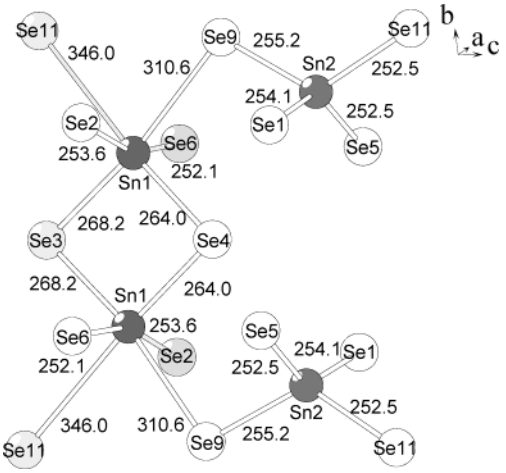

Figure 2. The "C-shaped" $Sn_4Se_{14}^{12-}$ unit of Sr_2SnSe_5. Gray: Sn. White: Se. Different heights are reflected in different shading.

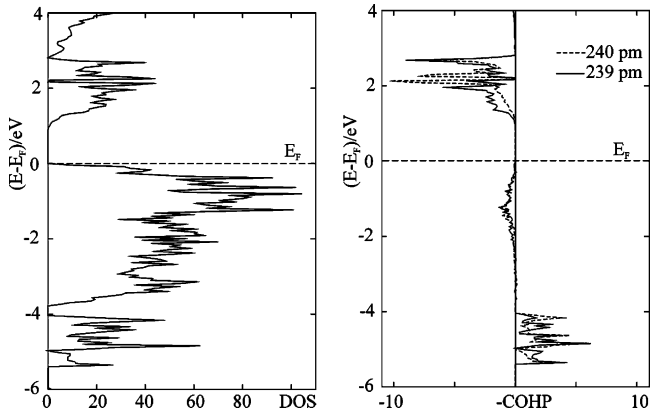

Figure 3. Densities of states (left) and Se−Se COHP curves (right) of Sr_2SnSe_5.

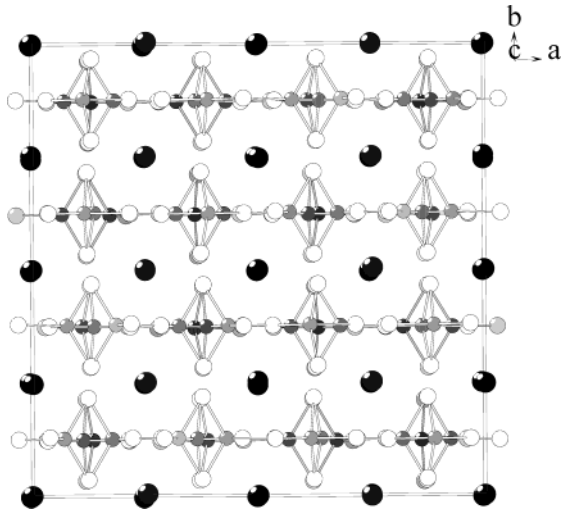

Figure 4. Projection of the structure of $SrSn_2Se_4$ along the *c* axis. Black circles: Sr. Gray: Sn. White: Se. Different heights are reflected in different shading; Sr−Se bonds are omitted for clarity.

it too may have a measurable impact. Such a coordination polyhedron is more commonly observed in Sb^{III} selenides that have a sterically active inert pair; e.g., Sb_2Se_3.[48] Similarly, Sn^{II} in SnSe comprises a 3 + 3 coordination with three distances between 274 and 279 pm and three longer ones of 334−347 pm.[49] Alkaline seleno-stannates with 5-fold coordination for Sn^{IV} are known to exhibit distances in a wide range as well, e.g., in $K_2Sn_2Se_5$ (Sn−Se distances of 251−286 pm)[50] and in $Cs_2Sn_3Se_7$ (249−280 pm).[51] It is concluded that distorted environments for Sn^{IV} are not that uncommon, despite the absence of an inert pair.

The Sn−Se polyhedra are interconnected to a "C-shaped" unit comprising four Sn atoms.[28] The $Sn(2)Se_4$ tetrahedron shares a corner with the (severely distorted) $Sn(1)Se_6$ "octahedron". Two of the latter are condensed by sharing a common edge made by the Se(3) and Se(4) atoms, which lie on the 2-fold rotation axis (Figure 2). If one includes the (likely nonbonding) Sn(2)−Se(11) contact of 346 pm, these C motifs form an infinite chain along the *c* axis, interconnected via the Se(11) atoms forming a short bond to Sn(2) (253 pm) and the long 346 pm distance.

We calculated the densities of states (DOS) of Sr_2SnSe_5 to analyze why this selenide is black, i.e., exhibits a band gap smaller than 1.7 eV (if any). To verify our initial assumption that the polyselenide group is responsible for the band gap size, we calculated the crystal orbital Hamilton population (COHP) curves[52] for both Se−Se bonds of the Se_3^{2-} unit. Like the well-established crystal orbital overlap population (COOP) curves[53] usually extracted from extended Hückel calculations, the COHP curves indicate at which energy range an interaction is bonding (depicted on the right side of the diagram) or antibonding. Figure 3 compares the DOS and the Se−Se COHP curves. The presence of a band gap (at the Fermi level) is obvious, and its size of 0.9 eV is in agreement with the experimentally observed black appearance, and comparable to the gap of 1.07 eV experimentally determined for Eu_2SnSe_5. Noting that this computational method underestimates band gaps by (arguably) 10−30% on average,[54,55] we estimate the gap to be between 1.0 and 1.2 eV.

The energy window shown is dominated by Se p states. At the bottom, between −5.5 and −4 eV, the contributions to the DOS almost exclusively stem from Se−Se bonding states, as a comparison with the Se−Se COHP curves reveals. The huge peak above this (between −4 and 0 eV) has predominantly nonbonding Se p character (composed of all Se atoms), including slightly antibonding states of the Se_3^{2-} unit. The Fermi level, arbitrarily placed at 0 eV, separates these filled states from the empty Se−Se antibonding states occurring between +0.9 and +2.8 eV. We conclude that these antibonding states are ultimately causing the black color (gap smaller than 1.7 eV), for they clearly domi-

(48) Voutsas, G. P.; Papazoglou, A. G.; Rentzeperis, P. J. *Z. Kristallogr.* **1985**, *171*, 261−268.
(49) Wiedemeier, H.; von Schnering, H. G. *Z. Kristallogr.* **1978**, *148*, 295−303.
(50) Klepp, K. O. *Z. Naturforsch.* **1992**, *47B*, 197−200.
(51) Sheldrick, W. S.; Braunbeck, H. G. *Z. Naturforsch.* **1990**, *45B*, 1643−1646.
(52) Dronskowski, R.; Blöchl, P. E. *J. Phys. Chem.* **1993**, *97*, 8617−8624.
(53) Hughbanks, T.; Hoffmann, R. *J. Am. Chem. Soc.* **1983**, *105*, 3528−3537.
(54) Yanagi, H.; Inoue, S.-I.; Ueda, K.; Kawazoe, H. *J. Appl. Phys.* **2000**, *88*, 4159−4163.
(55) Tampier, M.; Johrendt, D. *Z. Anorg. Allg. Chem.* **2001**, *627*, 312−320.

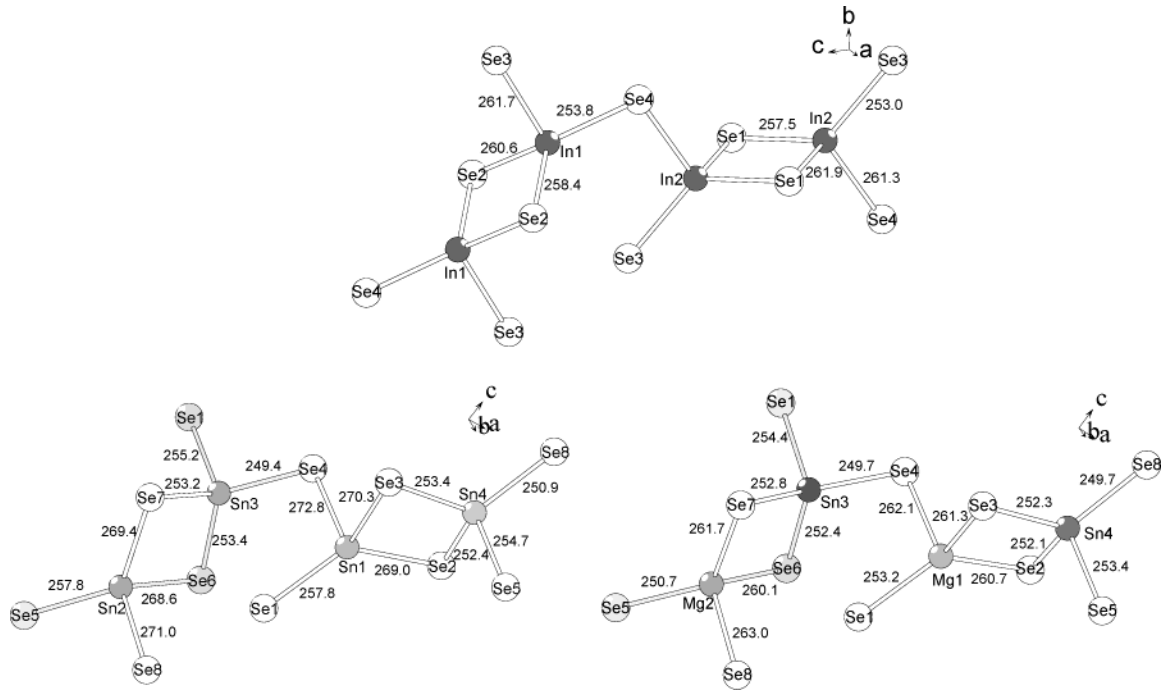

Figure 5. The repeating units of the infinite $E_4Se_8^{4-}$ layers (E = In, Sn, Mg) of $SrIn_2Se_4$ (top), $SrSn_2Se_4$ (bottom, left), and $SrMgSnSe_4$ (bottom, right).

nate the first peak above the Fermi level. The next peak starts around 2.6 eV, and the energy difference to the Fermi level would correspond to absorption of visible light.

To investigate how far the longer Sn−Se distances >300 pm are bonding, we analyzed their COHP curves. One can get a measure of the bond strength by integrating over all states of the COHP curve below the Fermi level. This procedure yielding the ICOHP value is related to extracting the Mulliken overlap populations (MOP)[56] from crystal orbital overlap populations (COOP).[53] ICOHP values differ from MOP values in their sign (negative ICOHP values indicate bonding character) and units (electronvolts per bond vs electrons per bond). As demonstrated before,[39,57,58] the absolute ICOHP values are typically higher than the corresponding MOP values (ignoring the different units). The Se−Se bonds exhibit rather large ICOHP values, namely, −2.66 eV for the 239 pm bond, and −2.53 eV for the 240 pm bond, indicative of strong bonding character.

The ICOHP values of the Sn(1)−Se interactions decrease exponentially with increasing distance, which is indicative of a strong bond length−bond strength correlation. The interaction of 311 pm can still be considered bonding, albeit significantly weaker than the shorter Sn−Se bonds, with an ICOHP value of −0.43 eV, compared to −1.80 eV for the 268 pm and −2.80 eV for the 252 pm interaction. The last one compares well to the ICOHP values of the short Sn(2)−Se bonds, which range from −2.94 to −2.58 eV/bond. On the other hand, since the ICOHP value of −0.09 for the 346 pm distance is only about 3% of the strongest Sn−Se interaction, that contact is best regarded as nonbonding. From that point of view, the coordination sphere of Sn(1) is to be described as 5-fold, comparable to the Sn atoms of $K_2Sn_2Se_5$ and $Cs_2Sn_3Se_7$, and the "C-shaped" unit comprising four Sn atoms is a finite tetramer.

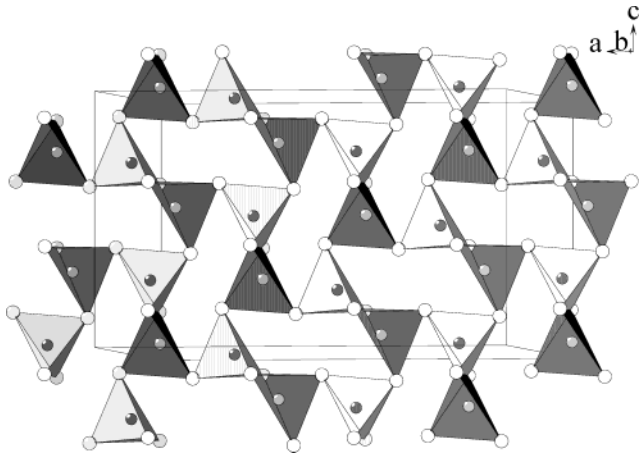

Figure 6. Polyhedral representation of the infinite $Sn_4Se_8^{4-}$ layer of $SrSn_2Se_4$. Dark polyhedra: Sn^{II}-centered. Bright: Sn^{IV}-centered.

The Isostructural Selenides $SrSn_2Se_4$ and $SrMgSnSe_4$. A projection of the structure of $SrSn_2Se_4$ is given in Figure 4, the Sr−Se bonds again being omitted. The Sr atoms form a secondary regular 4^4 net of linear chains (albeit without Sr−Sr interactions). The selenostannate groups form extended layers perpendicular to the *b* axis, separated from one another by the Sr atoms.

Since there are no Se−Se bonds in these two selenostannates, a straightforward assignment of oxidation state unambiguously yields $Sr^{II}Mg^{II}Sn^{IV}(Se^{-II})_4$. For $SrSn_2Se_4$, one could postulate either two Sn^{III} (like the two In^{III} in the aristotype $SrIn_2Se_4$) or mixed valent Sn, i.e., one Sn^{II} and one Sn^{IV}. The structure of $SrIn_2Se_4$ contains two symmetry independent In sites, which exhibit very similar 4-fold coordination, both with In−Se bonds of 253−262 pm (averaged 258.6 and 258.4 pm,

(56) Mulliken, R. S. *J. Chem. Phys.* **1955**, *23*, 2343−2346.
(57) Lee, C.-S.; Kleinke, H. *Eur. J. Inorg. Chem.* **2002**, 591−596.
(58) Dashjav, E.; Kleinke, H. *J. Solid State Chem.* **2003**, *176*, 329−337.

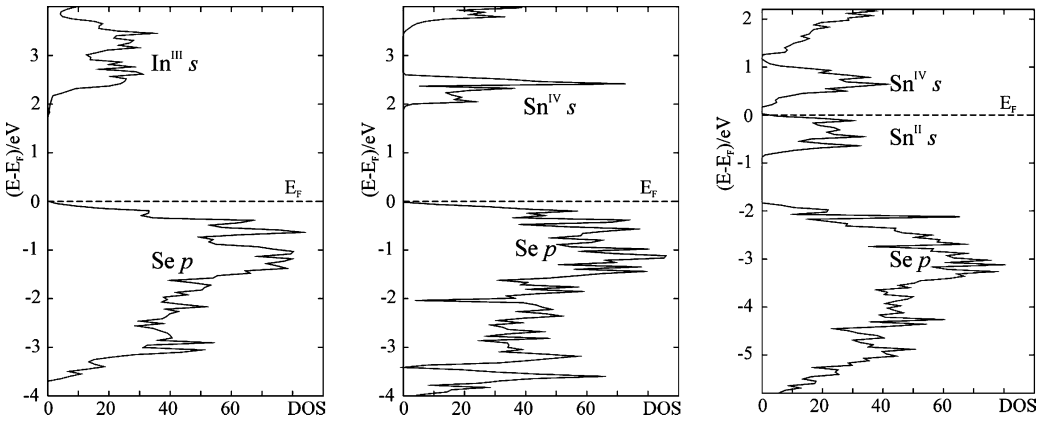

Figure 7. Densities of states of $SrIn_2Se_4$ (left), $SrMgSnSe_4$ (center), and $SrSn_2Se_4$ (right).

Table 6. Selected Interatomic Distances [pm] of $SrSn_2Se_4$ and $SrMgSnSe_4$

$SrSn_2Se_4$		$SrMgSnSe_4$	
Sn(1)−Se(1)	257.81(13)	Mg(1)−Se(1)	253.2(3)
Sn(1)−Se(2)	268.96(18)	Mg(1)−Se(2)	260.7(4)
Sn(1)−Se(3)	270.31(17)	Mg(1)−Se(3)	261.3(4)
Sn(1)−Se(4)	272.78(14)	Mg(1)−Se(4)	262.1(3)
Sn(2)−Se(5)	257.80(14)	Mg(2)−Se(5)	250.7(3)
Sn(2)−Se(6)	268.65(18)	Mg(2)−Se(6)	260.1(4)
Sn(2)−Se(7)	269.44(18)	Mg(2)−Se(7)	261.7(4)
Sn(2)−Se(8)	270.98(13)	Mg(2)−Se(8)	263.0(3)
Sn(3)−Se(4)	249.38(14)	Sn(3)−Se(4)	249.69(11)
Sn(3)−Se(7)	253.22(16)	Sn(3)−Se(6)	252.38(14)
Sn(3)−Se(6)	253.43(16)	Sn(3)−Se(7)	252.79(14)
Sn(3)−Se(1)	255.22(12)	Sn(3)−Se(1)	254.37(10)
Sn(4)−Se(8)	250.94(14)	Sn(4)−Se(8)	249.70(12)
Sn(4)−Se(2)	252.38(16)	Sn(4)−Se(2)	252.10(13)
Sn(4)−Se(3)	253.36(16)	Sn(4)−Se(3)	252.28(13)
Sn(4)−Se(5)	254.69(12)	Sn(4)−Se(5)	253.45(10)

respectively). The removal of the inversion center when going from $SrIn_2Se_4$ in *Fddd* to $SrSn_2Se_4$ in the subgroup *Fdd*2 leads to four independent Sn sites (Figure 5).

All Sn sites of $SrSn_2Se_4$ are coordinated by four Se atoms in approximately tetrahedral coordination. These four independent $SnSe_4$ tetrahedra are interconnected by sharing edges and corners to infinite layers, as the polyhedral representation in Figure 6 reveals. Two Sn sites show the typical Sn^{IV}−Se distances averaging slightly above 250 pm (Sn(3), 249−255 pm; Sn(4), 251−255 pm), and two sites significantly larger distances of 258−273 pm (Sn(1)) and 258−271 pm (Sn(2)) (Table 6). We therefore assign the oxidation states of the latter two to be +II, and thus conclude that $SrSn_2Se_4$ is indeed a mixed valent compound.

Very few solid-state seleno-stannates are known with the same mixed oxidation states (i.e., possibly Sn^{III}, or Sn^{II}/Sn^{IV}). $K_6Sn_2Se_6$ contains Sn^{III}, which is tetrahedrally coordinated by three Se atoms (251−252 pm) and another Sn^{III} atom, resulting in an $Sn_2Se_6^{6-}$ unit with a Sn−Sn single bond of 278 pm.[59] One mixed valent example is $Rb_2Sn_4Se_8$,[60] which contains three Sn^{IV} sites as well as one Sn^{II} site, the latter with four Se neighbors at distances between 272 and 315 pm. The Sn^{II} site in $Sn^{II}Se$[49] is bonded to six Se atoms at three short (274−279 pm) and three longer (334−347 pm) distances, showing a sterically active inert pair. In the case of $SrSn_2Se_4$, the $Sn^{II}Se_4$ tetrahedra are less distorted than in $Rb_2Sn_4Se_8$ and SnSe, with bond angles ranging from 94° to 129°, but more distorted than the $Sn^{IV}Se_4$ tetrahedra in $SrSn_2Se_4$.

The averaged Sn−Se distances of $SrSn_2Se_4$ are 267.5 pm for Sn(1), 266.7 pm for Sn(2), and 252.8 pm for Sn(3) as well as Sn(4). The two unambiguously tetravalent Sn atoms of $SrMgSnSe_4$ have averaged Sn−Se bonds of 252.3 pm (Sn(3)) and 251.9 pm (Sn(4)), respectively, and the Mg^{II} atoms exhibit averaged Mg−Se bonds of 259.4 pm (Mg(1)) and 258.9 pm (Mg(2)), respectively. The latter distances compare well with the averaged Mg−Se bond length (257.6 pm) of the tetracoordinated Mg^{II} atoms in $MgIn_2Se_4$.[61]

It is instructive to compare the electronic structures of $SrIn_2Se_4$, $SrMgSnSe_4$, and $SrSn_2Se_4$. Their projections onto the densities of states are illustrated in Figure 7. In all three cases, we chose an energy window of 8 eV so that the tops of the large Se p dominated peaks line up. Then, this peak occupies approximately the lowest 4 eV in all three cases. In the electronic structures of the colored selenides $SrIn_2Se_4$ and $SrMgSnSe_4$, the Se p peak is the highest occupied one, and a gap of 1.7 and 1.8 eV separates the filled states from the empty In^{III} s and Sn^{IV} s states, respectively. In light of the observed red color of $SrMgSnSe_4$, corresponding to a gap of approximately 2.0 eV, the calculated gap is underestimated by 10%, which is not untypical for this calculation method.[54,55]

On the other hand, we find the filled Sn^{II} s states between the empty Sn^{IV} s states and the filled Se p block in $SrSn_2Se_4$. This strongly supports our arguments favoring mixed valent Sn atoms instead of Sn^{III}. The Fermi level of $SrSn_2Se_4$ lies between the Sn^{II} s states and the empty Sn^{IV} s states, which are separated by a small gap of 0.2 eV. Such a gap would be ideal for the thermoelectric energy conversion.[25] To understand the different energies of the Sn^{II} and Sn^{IV} s states, we note that they are of antibonding Sn−Se character. (Their respective bonding Se-centered counterparts are found well below the Fermi level.) Since the Sn^{IV}−Se bonds are shorter, the antibonding states are raised higher in energy.

(59) Zimmermann, C.; Dehnen, S. *Z. Anorg. Allg. Chem.* **1999**, *625*, 1963−1965.
(60) Klepp, K. O.; Fabian, F. *Eur. Crystallogr. Meet.* **1994**, *15*, 626−626.
(61) Range, K.-J. *Z. Naturforsch.* **1996**, *51B*, 1363−1364.

Summary

We demonstrated that the band gaps can be minimized in seleno-stannates by using mixed valent Sn or Se atoms. Compounds with all atoms in the common oxidation states (i.e., Sn^{IV} and Se^{-II}) exhibit large band gaps that often cause intense colors, as observed for the red $SrMgSnSe_4$ (and the sulfide Sr_2SnS_4). On the other hand, Sr_2SnSe_5 with Sn^{IV}, Se^{-II}, and a classical Se_3^{2-} group containing $Se^{\pm 0}$ and Se^{-I} has a computed gap of 0.9 eV, and is black. The latter is also true for the mixed valent $SrSn_2Se_4$ that exhibits a computed gap of 0.2 eV between the states dominated by the Sn^{II} s contributions and those stemming from Sn^{IV} s. Structurally the Sn^{II} sites can readily be identified because of their larger distances to the neighboring Se atoms, compared to the Sn^{IV} sites. This difference between the Sn sites is the cause for the symmetry reduction expressed in going from the aristotype's ($SrIn^{III}_2Se_4$) space group *Fddd* to its subgroup *Fdd*2.

Acknowledgment. Financial support from NSERC, CFI, OIT (Ontario Distinguished Researcher Award for H.K.), the Province of Ontario (Premier's Research Excellence Award for H.K.), and the Canada Research Chair program (CRC for H.K.) is appreciated.

Supporting Information Available: Three X-ray crystallographic files (CIF). This material is available free of charge via the Internet at http://pubs.acs.org.

CM0499242